FULL PAPER

Enhancing the Angular Sensitivity of Plasmonic Sensors Using Hyperbolic Metamaterials

Kandammathe Valiyaveedu Sreekanth,* Yunus Alapan, Mohamed ElKabbash, Amy M. Wen, Efe Ilker, Michael Hinczewski, Umut A. Gurkan, Nicole F. Steinmetz, and Giuseppe Strangi*

Surface plasmon resonance (SPR) sensors operate mainly on prism and grating coupling techniques, with spectral and angular scans being the two major interrogation schemes. Among them, the angular scan technique has several advantages including higher measurement precision owing to its higher signal-to-noise ratio. The currently available SPR sensor arrangements provide a maximum angular sensitivity of 500°–600° per RIU. Here, we report the study of grating coupled-hyperbolic metamaterial (GC-HMM) sensors with high angular sensitivity. The experimental studies show extraordinary angular sensitivities from visible to near infrared (NIR) wavelengths by exciting bulk plasmon polaritons associated with hyperbolic metamaterials, with a maximum of 7000° per RIU. This angular-scan plasmonic biosensor has been used for the detection of low molecular weight biomolecules such as biotin (244 Da) and high molecular weight macromolecules such as Cowpea mosaic virus (CPMV, 5.6×10^6 Da) at ultralow concentrations. The miniaturized sensing device can be integrated with microfluidic systems for the development of next-generation biosensors for lab-on-a-chip and point-of-care applications.

1. Introduction

Surface plasmon polariton (SPP) based sensors have emerged as a promising technology for the development of next-generation biological and chemical sensors for high-throughput, label-free, and multianalyte sensing applications.[1–5] SPPs are collective charge density oscillations occurring at the interface between a metal and a dielectric that have been widely used for the investigation of change in refractive index near the metal–dielectric interface. This is because the electric field associated with these oscillations is very intense at this interface and decays exponentially in both interfacing media. Based on the momentum matching condition required for the excitation of SPP on a thin metal film, the SPP sensors are classified into two configurations: attenuated total-reflection (Kretschmann) and grating

Dr. K. V. Sreekanth, Dr. M. ElKabbash, Dr. E. Ilker, Prof. M. Hinczewski, Prof. G. Strangi
Department of Physics
Case Western Reserve University
10600 Euclid Avenue, Cleveland, OH 44106, USA
E-mail: sreekanth3@gmail.com; giuseppe.strangi@case.edu

Dr. A. M. Wen, Prof. U. A. Gurkan, Prof. N. F. Steinmetz
Biomedical Engineering Department
Case Western Reserve University
Cleveland, OH 44106, USA

Dr. Y. Alapan, Prof. U. A. Gurkan
Case Biomanufacturing and Microfabrication Laboratory
Mechanical and Aerospace Engineering Department
Case Western Reserve University
Cleveland, OH 44106, USA

Prof. U. A. Gurkan
Department of Orthopaedics
Case Western Reserve University
Cleveland, OH 44106, USA

Prof. U. A. Gurkan
Advanced Platform Technology Center
Louis Stokes Cleveland Veterans Affairs Medical Center
Cleveland, OH 44106, USA

Prof. N. F. Steinmetz
Department of Radiology
Case Western Reserve University
Cleveland, OH 44106, USA

Prof. N. F. Steinmetz
Department of Materials Science and Engineering
Case Western Reserve University
Cleveland, OH 44106, USA

Prof. N. F. Steinmetz
Department of Macromolecular Science and Engineering
Case Western Reserve University
Cleveland, OH 44106, USA

Prof. N. F. Steinmetz, Prof. G. Strangi
Case Comprehensive Cancer Center
Case Western Reserve University
Cleveland, OH 44106, USA

Prof. G. Strangi
Department of Physics and CNR-NANOTEC UOS of Cosenza
Licryl Laboratory
University of Calabria
87036 Rende, Italy

coupling.[6–9] In both configurations, two major interrogation schemes have been employed for acquiring the information by measuring the reflected signal: spectral scan and angular scan interrogation.[9–12] In spectral interrogation, the resonant wavelength shift in the reflectance spectrum indicates the refractive index change caused by the capture of biomolecules at the sensor surface, whereas angular shift is the indication of refractive index change in angular interrogation. In contrast to the spectral interrogation scheme, the main advantage of angular interrogation is that a single wavelength laser source is used rather than polychromatic light. Therefore, it is possible to achieve higher signal-to-noise ratio owing to the wavelength and power stability of the source. Thus, angular interrogation has been widely used in SPP sensors based on grating coupling and Kretschmann configurations.[12–15] Recently, a SPR arrangement based on angular interrogation has been used for the detection and quantification of bacteria.[16] An angular sensitivity maximum of up to 500°–600° per RIU has been theoretically reported using the Kretschmann configuration.[15] However, it is not possible to develop a miniaturized sensor device for lab-on-a-chip and point-of-care applications using the Kretschmann configuration due to the bulky end instrumentations required.[2]

Recently, advanced lithography techniques have made it possible to fabricate sub-wavelength metal gratings suitable for SPP sensors.[17–19] The primary advantage of metal nanograting-based SPP sensors is miniaturization, enabling lab-on-a-chip commercial applications such as antigen-antibody, protein, and chemical detection. To date, a maximum angular sensitivity of around 500° per RIU was reported using grating SPP sensors.[20] The angular sensitivity mainly depends on the incident wavelength, prism material, and the diffraction orders. Therefore, it remains challenging to achieve higher angular sensitivity (above 500° per RIU) using conventional (Kretschmann and grating) SPR sensor arrangements. To overcome these technological hurdles and push the limit of angular sensitivity of SPP sensors, we report a miniaturized plasmonic sensor geometry, which is a combination of a sub-wavelength metallic diffraction grating and a hyperbolic metamaterial.

Hyperbolic metamaterials (HMMs) are distinguished as a promising class of optical metamaterials, with bulk 3D subwavelength structures that are anisotropic in permittivity.[21] HMMs in the form of metal nanorods in a dielectric host (Type I) and ultrathin metal-dielectric multilayers (Type II) have several advantages, including 3D nonresonant optical responses with low loss. These nonmagnetic media have optical hyperbolic iso-frequency surfaces with a diagonal form of the permittivity tensor ($\varepsilon = \mathrm{diag}(\varepsilon_x, \varepsilon_y, \varepsilon_z)$) in which diagonal elements have different signs ($\varepsilon_x = \varepsilon_y$ and $\varepsilon_x . \varepsilon_z < 0$) leading to a hyperbolic dispersion $\omega^2/c^2 = (k_x^2 + k_y^2)/\varepsilon_z + k_z^2/\varepsilon_x$. Since HMM supports high-wavevector propagating modes (high-k modes), it promises a variety of potential applications such as spontaneous emission enhancement, nanoimaging, negative refraction, and perfect absorption.[22–28] It has also been recently demonstrated that a HMM can be used for the development of ultrasensitive plasmonic biosensors.[29,30] A plasmonic nanorod metamaterial (Type I HMM) has been proposed for high-sensitivity plasmonic biosensors with an extreme spectroscopic sensitivity of 32 000 nm per RIU and a figure of merit (FOM) of

330 at NIR frequencies.[29] In addition, a metal-dielectric stack-based HMM (Type II HMM) has been proposed for the realization of a miniaturized biosensor with many highly sensitive resonant modes from visible to NIR frequencies, with a reported maximum spectroscopic sensitivity of 30 000 nm per RIU and a record FOM of 590 at NIR wavelengths.[30] In both HMM-based biosensors, the ultrahigh spectroscopic resolution was achieved by exciting the high-k modes associated with HMMs. In the present work, we demonstrate that a metal-dielectric stack-based HMM can also be used for accomplishing extreme angular sensitivity by exciting the high-k modes of the HMM using a grating coupling technique. Since this plasmonic platform supports many modes from visible to NIR wavelengths, we report different extreme angular sensitivities for the range, with a maximum of 7000° per RIU at NIR and a minimum of 2000° per RIU at visible wavelengths. Performance of the sensor was evaluated using both low and high molecular weight biomolecules, i.e., biotin and CPMV. The relevance of using these two specific biomolecules is mainly based on unmet clinical needs to detect ultralow molecular weight proteins (like biotin) in cancer research. Very early, circulating tumor cells overexpress small proteins (<500 Da) that are extremely difficult to detect with currently available sensing technologies. Whereas the CPMV is a plant virus that we chose as a safe model system to mimic infectious disease. The 2014 Ebola epidemic as well as the 2015 Zika virus outbreak highlight the urgent need for detection and control of infectious diseases. With no approved treatments and preventative vaccines, detection, and monitoring are the first steps toward confinement and eradication of the spread of these and other infectious diseases.

2. Design and Fabrication

As we reported before,[31,32] a grating coupling technique was used to excite the bulk plasmon polaritons associated with the HMM. To accomplish this, a metallic diffraction grating-coupled HMM (GC-HMM) was fabricated (**Figure 1**a) and proposed to function as an ultrasensitive plasmonic biosensor. The designed HMM consisted of 16 alternating thin films of gold and aluminum dioxide (Al_2O_3) that were fabricated by layer-by-layer deposition of Al_2O_3 and gold thin films on a glass substrate using electron-beam evaporation of Al_2O_3 pellets and the thermal evaporation of gold pellets, respectively (see Supporting Information). The sensor device is based on the coupling condition between grating surface modes and bulk plasmon polariton (BPP) modes, allowing one to observe a change in resonance angle as the refractive index of the surrounding medium changes. This is due to the variation in coupling condition between these two modes because BPPs are the entire family of gap plasmon modes of the metal-dielectric stack.

The optical constants and the thickness of both grown thin films were determined using a variable-angle spectroscopic ellipsometer. The metallic filling ratio was around 35%, with individual gold and Al_2O_3 thicknesses of 16 and 30 nm, respectively. For the fabrication of GC-HMM, a thin spacer layer (Al_2O_3) of thickness 10 nm was first deposited on the HMM to improve the coupling between diffraction grating and HMM. An array of subwavelength holes with square lattice symmetry

www.MaterialsViews.com

ADVANCED
OPTICAL
MATERIALS
www.advopticalmat.de

FULL PAPER
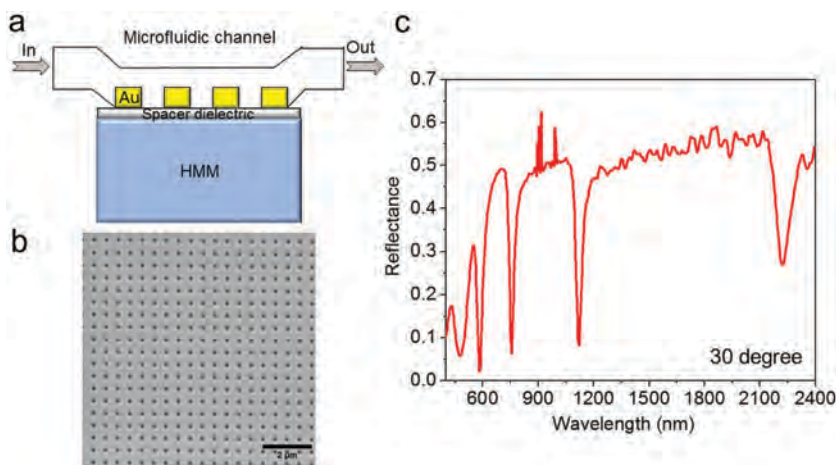
Figure 1. Design and characterization. a) Schematic representation of microfluidic channel integrated with grating coupled-HMM biosensor. b) SEM image of 2D gold hole array diffraction grating on top of the HMM (period = 500 nm and hole diameter = 160 nm). c) Reflectance spectrum of grating coupled-Au/Al₂O₃ HMM at 30° angle of incidence (wavelength spectroscopic resolution was set to 2 nm).

was patterned on top of the spacer layer using electron-beam lithography. Using a two-layer photoresist coating, deep subwavelength gratings were realized. Then, a thin gold layer of 20 nm thickness was directly deposited on top of the sample using thermal evaporation to realize a gold diffraction grating. The metal diffraction grating was chosen to be gold because of the easier functionalization processes with biomolecules by using thiol-based surface chemistry.[33] Figure 1b shows a scanning electron microscope (SEM) image of the 2D gold diffraction grating on the HMM with an average period and hole diameter of 500 and 160 nm, respectively.

We then used effective medium theory (EMT) to determine the uniaxial dielectric tensor components of the fabricated HMM,[25] $\varepsilon_{\parallel} = \varepsilon_x = \dfrac{t_m \varepsilon_m + t_d \varepsilon_d}{t_m + t_d}$ and $\varepsilon_{\perp} = \varepsilon_z = \dfrac{\varepsilon_m \varepsilon_d (t_m + t_d)}{t_m \varepsilon_d + t_d \varepsilon_m}$, where ($\varepsilon_d$, t_d) and (ε_m, t_m) are the dielectric permittivity and thickness of Al₂O₃ and gold, respectively. EMT-derived permittivity components (Figure S1, Supporting Information) of the fabricated gold-Al₂O₃ multilayer confirmed a Type II HMM with hyperbolic dispersion at $\lambda \geq$ 520 nm (i.e., $\varepsilon_{\parallel} < 0$ and $\varepsilon_{\perp} > 0$). Reflectance spectra at oblique incidence were obtained using variable angle high-resolution spectroscopic ellipsometry. The reflectance spectrum of the GC-HMM obtained using p-polarized light is shown in Figure 1c. In the hyperbolic region ($\lambda > 520$ nm), four reflectance dips with high quality factor resonance were obtained, which represents the highly confined bulk plasmon polaritons.[30,31] These modes can be experimentally probed by studying the reflectance spectra as a function of
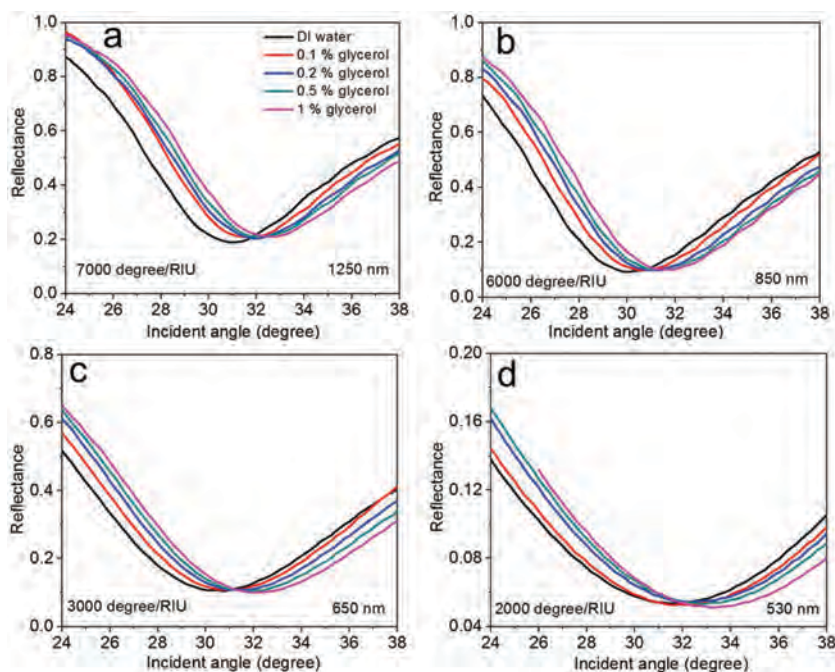
incident angle at a particular wavelength in each BPP mode band. As shown in **Figure 2**, the excitation of BPP modes in the four BPP bands with an equal bandwidth (50 nm) was investigated: 2100 to 2050 nm, 1100 to 1050 nm, 750 to 700 nm, and 550 to 500 nm. A decrease in resonance angle was observed when the excitation wavelength in each BPP band was increased, which indicates that the modal index of BPP modes decreases with an increase in excitation wavelength.[31,32] In particular, the resonance angle variation was different in each BPP wavelength band, with maximum for the shorter wavelength band (550 to 500 nm) and minimum for the longer wavelength band (2100 to 2050 nm). This is due to the fact that the modal index varies more at shorter wavelengths compared to longer wavelengths (Figure S2, Supporting Information). Also, the modal dispersion plot for surface and bulk plasmon modes is given in the Supporting Information (Figure S3).

Since the BPP modes showed different angular variation for each BPP wavelength band, it could be used to design a potential plasmonic biosensor with different angular sensitivities for each BPP wavelength band. Therefore, we fabricated a microfluidic channel integrated GC-HMM based miniaturized biosensor platform (see Supporting Information). For this purpose, a microfluidic system was assembled on top of the GC-HMM, which was composed of a poly(methyl methacrylate) plastic top (encompassing micromachined inlets and outlets) and a 50 μm
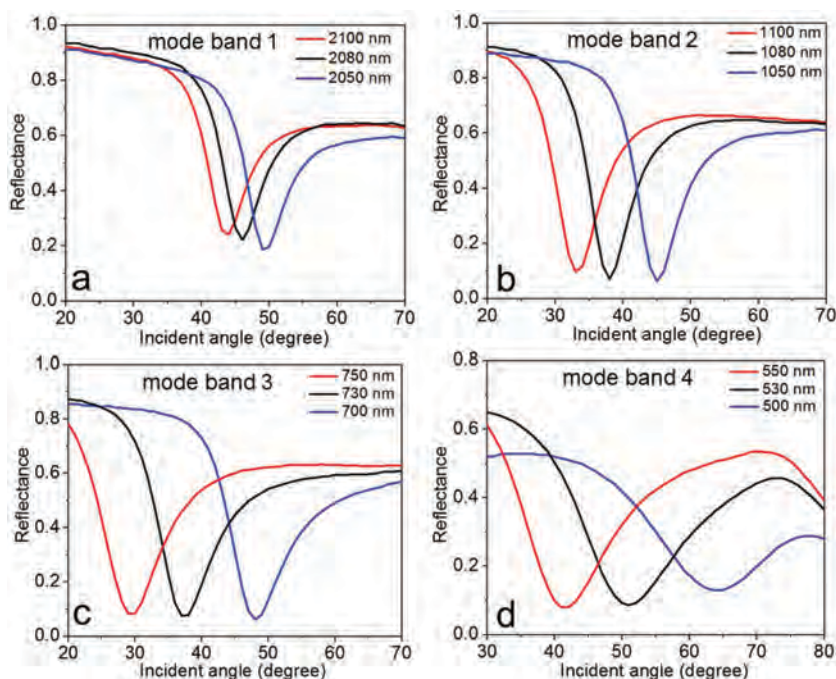
Figure 2. Excitation of bulk plasmon polaritons at four BPP mode bands. Reflectance spectra as a function of incident angle are shown for a) mode band 1 (2100–2050 nm), b) mode band 2 (1100–1050 nm), c) mode band 3 (750–700 nm), and d) mode band 4 (550–500 nm). The angular resolution of the instrument was set to 1°.

ADVANCED
OPTICAL
MATERIALS
www.advopticalmat.de

Materials
Views
www.MaterialsViews.com

FULL PAPER

Figure 3. Sensor evaluation using glycerol solutions. Reflectance spectra as a function of incident angle of the sensor device obtained by injecting different weight percentage concentration of glycerol in distilled water: a) at 1250 nm, b) at 850 nm, c) 650 nm, and d) 530 nm. A positive angular shift was observed when the glycerol weight percentage increased. The angular resolution of the instrument was set to 0.1°.

thick double sided adhesive film in the middle that defined the outline and the thickness of the microchannel.

3. Sensor Calibration Test

We first determined the angular detection limit of the sensor device by manually injecting different weight ratios (0.1%–1% (w/v)) of glycerol in the sensor flow microchannel. Here the aqueous solutions of glycerol were prepared in distilled (DI) water. The reflectance spectrum of the sensor device with DI water as the superstrate was first recorded (Figure S4, Supporting Information). Note that the longer wavelength BPP mode (at 2000 nm) was not present in the spectrum, in comparison to Figure 1c, which is due to the greater absorption capacity of the relatively thick PMMA channel at longer wavelengths. From the reflectance dip of the BPP mode bands, four resonant wavelengths were selected (1250, 850, 650, and 530 nm). In order to determine the angular sensitivity of the device, we recorded the reflectance spectra as a function of incident angle at each particular wavelength. The results obtained from injecting different weight ratios of glycerol in a sample volume of $14 \times 2 \times 0.05$ mm^3 are shown in **Figure 3**. One can see a positive angular shift for all four wavelengths when the glycerol weight ratio was increased from 0% to 1% (w/v). This shift represents the ability of the sensor to detect the extremely small refractive index change resulting from the change in glycerol concentration. Also note that the angular shift varied between the different modes. This is due to the fact that the transverse decay of the field in the superstrate strongly varies

from one mode to another.[30] In particular, the shift varied nonlinearly with glycerol concentration at the four wavelengths. This shows that the sensor has its highest performance at the lowest concentrations. Therefore, in order to determine the angular detection limit of the sensor, we calculated the angular sensitivity of the device at each BPP mode wavelength by considering the shift obtained at lowest concentration (0.1% (w/v) glycerol) (Figure S5, Supporting Information). The refractive index difference between DI water and 0.1% (w/v) glycerol in DI water is around 0.0001.[34] At 1250 nm wavelength, the obtained angular shift for 0.1% (w/v) glycerol was 0.7°, resulting in a calculated angular sensitivity for the refractive index change of 7000° per RIU (Figure 3a). The corresponding values at 850, 650, and 530 nm were (0.6° and 6000° per RIU), (0.3° and 3000° per RIU), and (0.2° and 2000° per RIU), respectively (Figure 3b–d). For 1% (w/v) glycerol, maximum angular shifts obtained were 1.6° at 1250 nm, 1.6° at 850 nm, 1.4° at 650 nm, and 1.8° at 530 nm. This shows that the angular sensitivity of BPP modes varies randomly with BPP mode band. This is because the diffraction orders of the sub-wavelength grating also decide the angular sensitivity of the sensor device. Note that the angular sensitivity of conventional grating SPR sensors behaves similarly.[9] Since the modal index of both BPP and SPP modes decrease with wavelength (Figure S2, Supporting Information), the angular sensitivity performance of BPP and SPP modes in relation to the wavelength should follow a similar pattern. In contrast to conventional SPP based sensors, all the BPP modes of GC-HMM show an improvement in angular sensitivity, with a maximum of 14-fold at 1250 nm and a minimum of 4-fold at 530 nm. Even though the angular sensitivity depends on the wavelength of incident light, here for the comparison purpose we assumed an angular sensitivity of 500° per RIU for SPP based sensors at all wavelengths. Since the sensor shows different angular sensitivities for each mode, there is flexibility in the selection of a particular mode for identification of specific biomolecules. In other words, there is the option of using a lower sensitivity mode for the detection of higher molecular weight biomolecules and a higher sensitivity mode for the detection of lower molecular weight biomolecules.

4. Sensing of Biomolecules

To demonstrate the capabilities of the presented device for the detection of biomolecules, angular detection was used for sensing low molecular weight biotin (molecular weight = 244 Da) and high molecular weight CPMV (molecular weight = 5.6×10^6 Da). For the capture of biotin, the streptavidin-biotin affinity model was used [see Supporting Information]. With this setup, our device was able to measure the refractive index
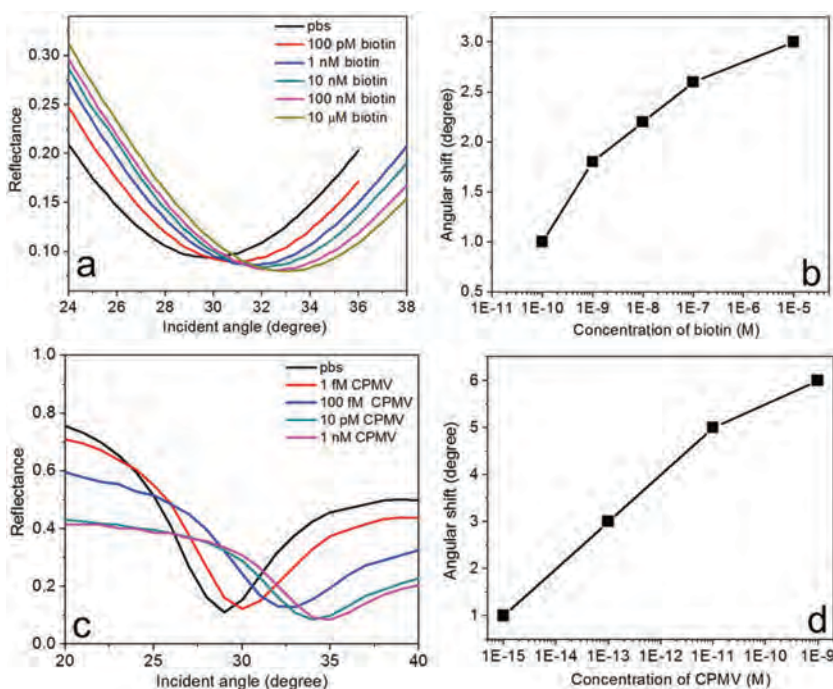
Figure 4. Angular detection of low and high molecular weight biomolecules at ultralow concentrations. a) Reflectance spectra of the sensor device at 1250 nm for different concentrations (100×10^{-12} M to 10×10^{-6} M) of biotin in PBS. b) The variation of angular shift with different concentrations of biotin. c) Reflectance spectra of the sensor device at 1250 nm for different concentrations (1×10^{-15} M to 1×10^{-9} M) of CPMV in PBS. b) The variation of angular shift with different concentrations of CPMV. Angular shift showed a distinct positive shift and nonlinear variation with increasing concentration. The angular resolution of the instrument was set to 0.1°. The size of the data points in (b) and (d) represent the error bar.

is a model system for small molecule compounds such as other vitamins, cancer-specific proteins, hormones, therapeutics, or contaminants such as pesticides or toxins.

We then performed experiments to detect high molecular weight macromolecules Cowpea mosaic virus. CPMV was propagated in and isolated from plants using methods described by Wen et al.[35] Different concentrations (1×10^{-15} M to 1×10^{-9} M) of CPMV were prepared in PBS and then injected into the sensor microchannel. PBS was injected into the channel to remove unbound and weakly attached CPMV before each injection of a new solution. After 20 min reaction time, the reflectance spectra for the highly diluted CPMV solutions were recorded (Figure 4c). A large angular shift of 1° was obtained for 1×10^{-15} M CPMV, whereas 1×10^{-9} M CPMV provided an angular shift of 6°. In addition, the binding of CPMV to the sensor surface was investigated by recording the reflectance spectrum over time (Figure S6, Supporting Information). Also in this case, we observed a nonlinear variation in angular shift with concentration. The sensor performance for the mode at 1250 nm is shown for different concentrations of CPMV in Figure 4d. Since the molecular weight of CPMV is very large, the sensor saturates very quickly when the concentration was increased up to 1×10^{-9} M.

We then determined the sensitivity of the angular shift to the number of adsorbed molecules on the sensor surface and the data points in Figure 4b,d were fitted using a double exponential function (Figure S7, Supporting Information). The sensitivity analysis indicates that for CPMV at 1×10^{-15} M concentrations there are at most eight particles on average adsorbed in the sensing region of the surface. Given the corresponding large angular shift of 1°, this suggests that our novel sensor system could possibly achieve single-molecule detection levels. Therefore, the BPP-based biosensor has potential to match the sensitivity of nucleic acid technology-based sensors, with the added advantage that biospecimen processing to remove the encapsulated RNA cargos would not be necessary.

The highly nonlinear response of the sensor to concentration is an intrinsic property of the device, and is consistently present across all the times scales we probed, even the longest where equilibrium was approximately achieved. We anticipate a further improvement in sensitivity for detection of lower molecular weight biomolecules through controlling the parameters of the GC-HMM device. This could be achieved by tuning the GC-HMM design, especially the diffraction grating geometry. In comparison to conventional biosensors based on SPPs or metamaterials, the presented system can provide different angular sensitivity modes in the visible to NIR range. Specificity to detect viruses in complex media (blood or other body fluids and tissue samples) need to be achieved for commercial implementation, and will be a future direction. In particular, we are investigating this by functionalizing the sensor surfaces

change caused by the capture of biotin at the sensor surface within the microfluidic channel. The performance of the sensor was monitored based on the resonant angular shift in the reflectance spectrum when different concentrations (100×10^{-12} M to 10×10^{-6} M) of biotin in phosphate buffered saline (PBS) were injected into the sensor microchannel. It should be noted that we have used a single injection procedure for all our measurements. We first recorded the reflectance spectrum of the sensor device by injecting PBS. We then injected different concentrations of biotin, and the corresponding reflectance spectra as a function of incident angle were recorded after a reaction time of 40 min. Before each injection of a new concentration of biotin, PBS was introduced into the microchannel to remove the unbound and weakly attached biotin molecules. Since the mode at 1250 nm showed maximum angular sensitivity, we used that particular mode to study the biomolecular binding on the streptavidin-functionalized sensor surface, as shown in **Figure 4**a. A positive angular shift was obtained when the biotin concentration was increased, which is due to the increase in refractive index by the capture of biomolecules. As shown in Figure 4b, a nonlinear variation in angular shift, as a function of the biotin concentration, was observed. In particular, a large angular shift of 1° was obtained for 100×10^{-12} M biotin, while the obtained angular shift for 10×10^{-6} M was only 3°. These results demonstrate that the presented device has the capability to detect low molecular weight biomolecules with a sensitivity of 100×10^{-12} M. We used biotin as a proof-of-concept—biotin

FULL PAPER

with antibodies, which can selectively capture specific proteins, viruses, or even entire cells.

5. Conclusions

In summary, a grating coupled-hyperbolic metamaterial biosensor with enhanced angular sensitivity was demonstrated. In contrast to existing biosensors based on SPPs, we achieved different extreme sensitivity modes with 14, 12, 6, and 4 times higher angular sensitivity by exciting the bulk plasmon polaritons of HMM at 1250, 850, 650, and 530 nm wavelengths, respectively. With our new biosensor, we demonstrated the angular detection of low molecular weight biomolecules such as biotin in highly diluted solutions using a standard streptavidin-biotin affinity model. In addition, the angular detection of high molecular weight biomolecules such as CPMV, a model virus particle, at concentrations as low as 1×10^{-15} M was demonstrated. Since angular interrogation scheme offers higher measurement precision as compared to spectral interrogation, this miniaturized sensing scheme can be used for the development of next-generation sensors for biomedical, environmental, and chemical applications.

Supporting Information

Supporting Information is available from the Wiley Online Library or from the author.

[1] J. N. Anker, W. P. Hall, O. Lyandres, N. C. Shah, J. Zhao, R. P. Van Duyne, *Nat. Mater.* **2008**, *7*, 442.

[2] A. G. Brolo, *Nat. Photonics* **2012**, *6*, 709.

[3] S. Zeng, D. Baillargeat, H. E. Hod, K.-T. Yong, *Chem. Soc. Rev.* **2014**, *43*, 3426.

[4] P. Zijlstra, P. M. R. Paulo, M. Orrit, *Nat. Nanotechnol.* **2012**, *7*, 379.

[5] S. Zeng, K. V. Sreekanth, J. Shang, T. Yu, C.-K. Chen, F. Yin, D. Baillargeat, P. Coquet, H.-P. Ho, A. V. Kabashin, K.-T. Yong, *Adv. Mater.* **2015**, *27*, 6163.

[6] J. Homola, S. S. Yee, G. Gauglitz, *Sens. Actuators, B* **1999**, *54*, 3.

[7] B. H. Huisman, R. P. H. Kooyman, F. C. J. M. ven Veggel, D. N. Reinhoudi, *Adv. Mater.* **1996**, *8*, 561.

[8] K. V. Sreekanth, S. Zeng, K.-T. Yong, T. Yu, *Sens. Actuators, B* **2013**, *182*, 424.

[9] J. Homola, I. Koudela, S. S. Yee, *Sens. Actuators, B* **1999**, *54*, 16.

[10] M. Lee, H. Jeon, S. Kim, *Nano Lett.* **2015**, *15*, 3358.

[11] D. Cai, Y. Lu, K. Lin, P. Wang, H. Ming, *Opt. Exp.* **2008**, *16*, 14597.

[12] H. R. Gwon, S. H. Lee, *Mater. Trans.* **2010**, *51*, 1150.

[13] M. T. Flanagan, R. H. Pantell, *Electron. Lett.* **1984**, *20*, 968.

[14] C. Nylander, B. Liedberg, T. Lind, *Sens. Actuators* **1982**, *3*, 79.

[15] D. W. Huang, Y.-F. Ma, M.-J. Sung, C.-P. Huang, *Opt. Eng.* **2010**, *49*, 054403.

[16] O. Tokel, U. Hakan, F. Inci, N. G. Durmus, O. O. Ekiz, B. Turker, C. Cetin, S. Rao, K. Sridhar, N. Natarajan, H. Shafiee, A. Dana, U. Demirci, *Sci. Rep.* **2015**, *5*, 9152.

[17] M. J. Joy, P. S. Vukusic, J. R. Sambles, *Sens. Actuators, B* **1994**, *17*, 203.

[18] D. C. Culle, R. G. W. Brown, C. R. Lowe, *Biosensors* **1987**, *3*, 211.

[19] C. R. Lawrence, N. J. Geddes, D. N. Furlong, J. R. Sambles, *Biosens. Bioelectron.* **1996**, *11*, 389.

[20] X. Sun, X. Shu, C. Chen, *Appl. Opt.* **2015**, *54*, 1548.

[21] A. Poddubny, I. Iorsh, P. Belov, Y. Kivshar, *Nat. Photonics* **2013**, *7*, 948.

[22] Z. Jacob, I. I. Smolyaninov, E. E. Narimanov, *Appl. Phys. Lett.* **2012**, *100*, 181105.

[23] K. V. Sreekanth, K. Hari Krishna, A. De Luca, G. Strangi, *Sci. Rep.* **2014**, *4*, 6340.

[24] A. J. Hoffman, L. Alekseyev, S. S. Howard, K. J. Franz, D. Wasserman, V. A. Podolskiy, E. E. Narimanov, D. L. Sivco, C. Gmachi, *Nat. Mater.* **2007**, *6*, 946.

[25] K. V. Sreekanth, A. De Luca, G. Strangi, *Appl. Phys. Lett.* **2013**, *103*, 023107.

[26] A. Ono, J. I. Kato, S. Kawat, *Phys. Rev. Lett.* **2005**, *95*, 267407.

[27] C. Guclu, S. Campione, F. Capolino, *Phys. Rev. B* **2012**, *86*, 205130.

[28] I. Avrutsky, I. Salakhutdinov, J. Elser, V. Podolskiy, *Phys. Rev. B* **2007**, *75*, 241402.

[29] A. V. Kabashin, P. Evans, S. Pastkovsky, W. Hendren, G. A. Wurtz, R. Atkinson, V. A. Podolskiy, A. V. Zayats, *Nat. Mater.* **2009**, *8*, 867.

[30] K. V. Sreekanth, Y. Alapan, M. ElKabbash, E. Ilker, M. Hinczewski, U. A. Gurkan, A. De Luca, G. Strangi, *Nat. Mater.* **2016**, *15*, 621.

[31] K. V. Sreekanth, A. De Luca, G. Strangi, *Sci. Rep.* **2013** *3*, 3291.

[32] K. V. Sreekanth, A. De Luca, G. Strangi, *J. Opt.* **2014**, *16*, 105103.

[33] P. Baptista, E. Pereira, P. Eaton, G. Doria, A. Miranda, P. Quaresma, R. Franco, *Anal. Bioanal. Chem.* **2008**, *391*, 943.

[34] U. S. Vural, V. Muradoglu, S. Vural, *Bull. Chem. Soc. Ethiop.* **2011**, *25*, 111.

[35] A. M. Wen, M. Infusino, A. De Luca, D. L. Kernan, A. E. Czapar, G. Strangi, N. F. Steinmetz, *Bioconjugate Chem.* **2015**, *26*, 51.